Nonlinear ARX (NARX) based identification and fault detection in a 2 DOF system with cubic stiffness

J.S. Sakellariou *and* **S.D. Fassois**
Stochastic Mechanical Systems (SMS) Group
Department of Mechanical & Aeronautical Engineering
e-mail: {sakj,fassois}@mech.upatras.gr
web page: http://www.mech.upatras.gr/∼sms

Abstract

This paper addresses the problem of system identification and fault detection in a two DOF nonlinear system characterized by cubic stiffness. System identification is based upon Nonlinear ARX (NARX) models, while a novel Functional Model Based Method is employed, for the first time within the context of a nonlinear system, for tackling the combined problem of fault detection, identification (localization), and fault magnitude estimation. The Functional Model Based Method utilizes Functional NARX (FNARX) models, which are capable of accurately representing the system in a faulty state for the latter's continuum of fault magnitudes, as well as statistical decision theory tools. The results of the study indicate the effectiveness of both NARX based identification and the Functional Model Based Method in detecting, identifying, and estimating the magnitude of faults based upon only two measured signals.

1 Introduction

This paper is concerned with the problems of system identification and fault detection, identification (localization), and magnitude estimation in a two DOF (Degree-of-Freedom) system characterized by local polynomial nonlinearity (cubic stiffness k_3; figure 1).

The approach postulated is based upon discrete-time *NARX models* [1, 2, 3], that is Nonlinear AutoRegressive models with eXogenous excitation, which constitute nonlinear extensions of the conventional linear ARX models [4, 5]. Unlike alternative nonlinear representations, such as those based upon Volterra or Wiener series [1, 6, 7], describing functions [1, 8], or neural networks [1], which are often used in identification, NARX models offer a number of advantages, including accuracy and compactness of representation (the latter leading to improved statistical parsimony), physical significance, and direct correspondence between the NARX and the physical system parameters. NARX models also feature linear regression based estimation and the availability of a number of tools for model structure selection [9].

Once the feasibility and effectiveness of NARX based system identification is demonstrated, the combined problem of fault detection, identificaton (localization), and magnitude estimation is tackled via a *Functional Model Based Method*. This method,

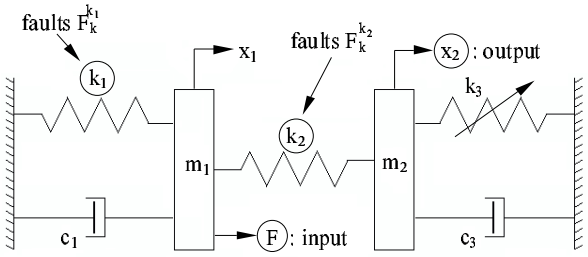

Figure 1: Two DOF system with cubic stiffness.

which has been recently introduced by the authors [10, 11], is used for the first time within the context of a nonlinear system, cultivating upon the NARX based system representation. The Functional Model Based Method achieves fault detection, identification, and magnitude estimation in a *unified* way, based upon the novel class of stochastic functional models and statistical decision theory tools. The stochastic functional models, presently *Functional NARX (FNARX) models*, play a very central role, as they are capable of accurately representing the system in a faulty state for the latter's continuum of fault magnitudes.

The rest of this paper is organized as follows: The system and the considered faults are described in section 2, while NARX based identification is presented in section 3. The Functional Model Based Method

$m_1 = 10$	$m_2 = 55$		(kg)
$k_1 = 10$	$k_2 = 90$	$k_3 = 900$	(kN/m)
$c_1 = 750$	$c_3 = 300$		(Ns/m)

Table 1: Physical system parameters.

Fault mode	Description
$F_k^{k_2}$	k_2 stiffness changes ($k = -32 \ldots 32\%$)
$F_k^{k_1}$	k_1 stiffness changes (reduction value $k = 30\%$)

Table 2: The considered fault modes.

for fault detection, identification, and magnitude estimation is presented in section 4, and corresponding results are summarized in section 5. The conclusions of this study are summarized in section 6.

2 The system and the faults

The two degree-of-freedom system considered is characterized by cubic stiffness in spring k_3 (figure 1). The rest of the system elements are linear. The system's physical parameters are indicated in table 1.

The system dynamics are described by the differential equations:

$$\begin{aligned} m_1 \cdot \ddot{x}_1 + (k_1 + k_2) \cdot x_1 - k_2 \cdot x_2 + c_1 \cdot \dot{x}_1 &= F \\ m_2 \cdot \ddot{x}_2 - k_2 \cdot x_1 + k_2 \cdot x_2 + k_3 \cdot x_2^3 + c_3 \cdot \dot{x}_2 &= 0 \end{aligned} \quad (1)$$

with F designating a force externally applied on mass m_1, and x_i, $\dot{x}_i$, $\ddot{x}_i$ the i-th mass displacement, velocity, and acceleration, respectively.

System identification and fault detection are both based upon measurement of the force excitation F (subsequently designated as x) and the vibration displacement response x_2 (subsequently designated as y).

System simulation is based upon discretization of equations (1) via forward differencing [12, pp.13-22] with time step $T_s = 6.666 \times 10^{-4}\ sec$ (sampling frequency $f_s = 1,500Hz$).

The faults. Two types of faults *(fault modes)* are considered (table 2 and figure 1): The first mode corresponds to stiffness changes in k_2. Each individual fault is represented as $F_k^{k_2}$, with the superscript k_2 indicating the fault mode and the subscript k the exact fault magnitude (changes in the range of $k = -32 \ldots 32\%$ are considered; negative/positive values indicate stiffening/loosening, respectively).

The second mode corresponds to stiffness changes in k_1. Each individual fault is similarly represented as $F_k^{k_1}$. A single fault mangitude of $k = 30\%$ (stiffness reduction) is in this case considered.

3 NARX based identification

The manipulation of the discretized system equations of motion leads to the following relationship between the force excitation $x[t]$ and the obtained displacement response $y[t]$[1]:

$$\begin{aligned} y[t] = \sum_{i=1}^{ma} a_i \cdot \varphi_i[t] + \sum_{i=1}^{mb} b_i \cdot \varphi_{ma+i}[t] \quad &\Longrightarrow \\ \Longrightarrow \quad y[t] \;=\; \boldsymbol{\varphi}^T[t] \cdot \boldsymbol{\vartheta} \end{aligned} \quad (2)$$

where:

$$\boldsymbol{\varphi}[t] \stackrel{\Delta}{=} [\varphi_1[t] \ldots \varphi_{ma+mb}[t]]^T_{[(ma+mb)\times 1]} \quad (3)$$

$$\boldsymbol{\vartheta} \stackrel{\Delta}{=} \left[a_1 \ldots a_{ma} \vdots b_1 \ldots b_{mb} \right]^T_{[(ma+mb)\times 1]} \quad (4)$$

and t designates normalized discrete time ($t = 1, 2, 3, \ldots$) with absolute time being $(t-1) \cdot T_s$.

The regressors $\varphi_i[t]$ $(i = 1, \ldots, ma + mb)$ are monomials of degrees $l = 1, 2, 3$, as indicated in table 3. With the addition of a zero mean, uncorrelated, and uncrosscorrelated with the excitation $x[t]$, noise term $e[t]$ in equation 2, the excitation-response relationship assumes the NARX(na,nb) (Nonlinear AutoRegressive with eXogenous excitation) form [1, 2]:

$$\boxed{y[t] \;=\; \boldsymbol{\varphi}^T[t] \cdot \boldsymbol{\vartheta} + e[t]} \quad (5)$$

In this form $\boldsymbol{\vartheta}$ represents the model parameter vector, with a_i $(i = 1, \ldots, ma)$ designating the i-th AR (AutoRegressive) parameter and b_i $(i = 1, \ldots, mb)$ the i-th X (eXogenous) parameter, and $na = 4$, $nb = 4$, the AR and X orders, respectively. The excitation-response delay (see the X term in table 3) is $d = 4$, while the model includes linear, quadratic, and cubic terms, with the maximum nonlinearity degree being max $l = 3$ (see table 3).

System identification. Identification of the healthy system is based upon the NARX(na,nb) model of the form of table 3. Estimation is accomplished via minimization of the quadratic criterion

[1] Lower case/capital bold face symbols designate vector/matrix quantities, respectively.

Degree		$l=1$		$l=2$		$l=3$
	Par.	Monomial	Par.	Monomial	Par.	Monomial
AR term	a_1	$\varphi_1[t] = y[t-1]$	a_5	$\varphi_5[t] = y[t-3] \cdot y[t-4]$	a_7	$\varphi_7[t] = y[t-2] \cdot y^2[t-4]$
" "	a_2	$\varphi_2[t] = y[t-2]$	a_6	$\varphi_6[t] = y^2[t-4]$	a_8	$\varphi_8[t] = y[t-3] \cdot y^2[t-4]$
" "	a_3	$\varphi_3[t] = y[t-3]$			a_9	$\varphi_9[t] = y^3[t-4]$
" "	a_4	$\varphi_4[t] = y[t-4]$				
X term	b_1	$\varphi_5[t] = x[t-4]$				
AR order: $na=4$		X order: $nb=4$		Delay: $d=4$		
AR terms: $ma=9$		X terms: $mb=1$				

Table 3: The NARX(na, nb) model structure.

$J_{NARX} = \frac{1}{N}\sum_{t=1}^{N} e^2[t]$, with N designating the length of the excitation-response signals used. Owing to the linear dependence of the error term $e[t]$ upon the parameter vector $\boldsymbol{\vartheta}$, this leads to the linear regression estimator:

$$\hat{\boldsymbol{\vartheta}} = \left(\frac{1}{N}\sum_{t=1}^{N} \boldsymbol{\varphi}[t] \cdot \boldsymbol{\varphi}^T[t]\right)^{-1} \cdot \left(\frac{1}{N}\sum_{t=1}^{N} \boldsymbol{\varphi}[t] \cdot y[t]\right) \quad (6)$$

$$\hat{\sigma}_e^2 = \frac{1}{N}\sum_{t=1}^{N} \hat{e}^2[t] \quad (7)$$

Identification is presently based upon $N = 30,000\ sample$ ($20\ sec$) long excitation and response signals. A typical vibration response signal is depicted in figure 2, whereas the corresponding identification result (model-based one-step-ahead predictions and prediction errors) is, for a segment of that signal, presented in figure 3. As it may be readily observed, the model-based predictions practically coincide with the system response and the prediction errors are very small.

4 The fault detection and identification method

The Functional Model Based Method consists of two phases (also see [10, 11]): The *first* (a-priori) phase includes the baseline modeling (via identification) of the healthy system's dynamics, as well as the modeling of each fault mode, for its continuum of fault magnitudes, via the novel class of *stochastic functional models*.

The *second* (inspection) phase is performed periodically during the system's service cycle, and includes the functions of fault detection, identification (localization), and fault magnitude estimation.

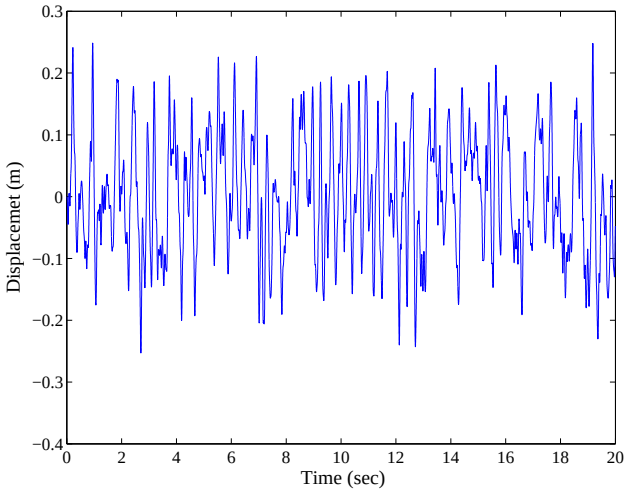

Figure 2: System vibration displacement response.

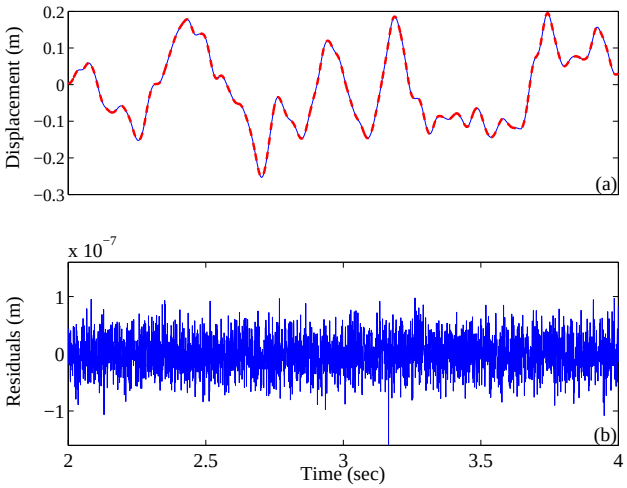

Figure 3: (a) The actual (—) and predicted (- - -) displacement responses; (b) the corresponding prediction errors.

4.1 Baseline and fault mode modeling (a-priori phase)

Baseline modeling. A single experiment is performed, based upon which an interval estimate of

a NARX(na, nb) dynamical model, of the form of equation (5) representing the healthy system's dynamics, is obtained.

Fault mode modeling. The notion of *fault mode* refers to the union of faults of all possible magnitudes (severities) originating from a single physical cause.

For the modeling of a fault mode, a series of M experiments are performed (either physically or via simulation). Each experiment is characterized by a specific fault magnitude k, with the complete series covering the range of possible fault magnitudes, say $[k_{min}, k_{max}]$, via a discretization $\{k_1, k_2, \ldots, k_M\}$ (in the sequel it is tacitly assumed, without loss of generality, that the healthy system corresponds to $k = 0$). This procedure yields a series of excitation-response signal pairs (each of length N):

$$x_k[t],\, y_k[t] \quad (t = 1, \ldots, N) \quad (k = k_1, k_2, \ldots, k_M) \tag{8}$$

Based upon these, a proper mathematical description of the fault mode may be constructed in the form of a stochastic Functional Model (presently Functional NARX – FNARX – model). A FNARX model, being a generalization of a NARX model (5), is of the form:

$$\boxed{\mathcal{M}(\overline{\boldsymbol{\theta}}): \quad y_k[t] = \boldsymbol{\varphi}_k^T[t] \cdot \boldsymbol{\vartheta}(k) + e_k[t] \quad k \in \mathbb{R}} \tag{9}$$

$$\boxed{\boldsymbol{\vartheta}(k) \;=\; \Big[a_1(k) \ldots a_{ma}(k) \vdots b_1(k) \ldots b_{mb}(k)\Big]^T} \tag{10}$$

$$\boxed{a_i(k) \stackrel{\Delta}{=} \textstyle\sum_{j=1}^{p} a_{ij} G_j(k) \quad b_i(k) \stackrel{\Delta}{=} \sum_{j=1}^{p} b_{ij} G_j(k)} \tag{11}$$

In these expressions k designates the fault magnitude, $\boldsymbol{\varphi}_k[t]$ is defined analogously to $\boldsymbol{\varphi}[t]$ [equation (3)], $x_k[t]$, $y_k[t]$ designate the corresponding measured excitation and resulting response signals, respectively, and $e_k[t]$ the corresponding stochastic model residual (one-step-ahead prediction error). For an accurate model, the residual sequence is zero-mean, uncorrelated, with variance $\sigma_e^2(k)$, and uncrosscorrelated with the corresponding excitation. Residual sequences corresponding to different fault magnitudes are assumed uncrosscorrelated.

As equation (11) indicates, the AR and X parameters $a_i(k)$, $b_i(k)$ are modeled as explicit functions of the fault magnitude k, belonging to a p-dimensional functional space spanned by the (mutually independent) functions $G_1(k), \ldots, G_p(k)$ (*functional basis*). The constants a_{ij}, b_{ij} designate the AR and X, respectively, coefficients of projection.

The FNARX model of equations (9)-(11), designated as $\mathcal{M}(\overline{\boldsymbol{\theta}})$, is thus parametrized in terms of the parameter vector (to be estimated from the measured signals):

$$\overline{\boldsymbol{\theta}} \stackrel{\Delta}{=} [\; a_{ij} \vdots b_{ij} \vdots \sigma_e^2(k) \;]^T \stackrel{\Delta}{=} \Big[\boldsymbol{\theta}^T \vdots \sigma_e^2(k)\Big]^T \qquad \forall i, j, k$$

The model of equation (9) may be then re-written as:

$$y_k[t] = \big[\boldsymbol{\varphi}_k^T[t] \otimes \boldsymbol{g}^T(k)\big] \cdot \boldsymbol{\theta} + e_k[t] = \boldsymbol{\phi}_k^T[t] \cdot \boldsymbol{\theta} + e_k[t] \tag{12}$$

with:

$$\boldsymbol{g}(k) \stackrel{\Delta}{=} [\, G_1(k) \ldots G_p(k) \,]^T_{[p \times 1]} \tag{13}$$

$$\boldsymbol{\theta} \stackrel{\Delta}{=} \Big[a_{1,1} \ldots a_{ma,p} \vdots b_{1,1} \ldots b_{mb,p}\Big]^T_{[(ma+mb)\cdot p \times 1]} \tag{14}$$

and $\otimes$ designating Kronecker product [13, pp. 27-28].

For model parameter estimation, the FNARX equation (12) gives, following substitution of the data [equation (8)] corresponding to a single fault magnitude k:

$$\begin{bmatrix} y_k[1] \\ \vdots \\ y_k[N] \end{bmatrix} = \begin{bmatrix} \boldsymbol{\phi}_k^T[1] \\ \vdots \\ \boldsymbol{\phi}_k^T[N] \end{bmatrix} \cdot \boldsymbol{\theta} + \begin{bmatrix} e_k[1] \\ \vdots \\ e_k[N] \end{bmatrix} \tag{15}$$

$$\Longrightarrow \; \boldsymbol{y}_k = \boldsymbol{\Phi}_k \cdot \boldsymbol{\theta} + \boldsymbol{e}_k \tag{16}$$

Stacking together these expressions for the data corresponding to the discrete fault magnitudes $\{k_1, k_2, \ldots, k_M\}$ considered in the experiments yields:

$$\boldsymbol{y} = \boldsymbol{\Phi} \cdot \boldsymbol{\theta} + \boldsymbol{e} \tag{17}$$

with:

$$\underbrace{\boldsymbol{y} \stackrel{\Delta}{=} \begin{bmatrix} \boldsymbol{y}_1 \\ \boldsymbol{y}_2 \\ \vdots \\ \boldsymbol{y}_M \end{bmatrix}}_{[NM \times 1]} \quad \underbrace{\boldsymbol{\Phi} \stackrel{\Delta}{=} \begin{bmatrix} \boldsymbol{\Phi}_1 \\ \boldsymbol{\Phi}_2 \\ \vdots \\ \boldsymbol{\Phi}_M \end{bmatrix}}_{[NM \times (ma+mb)\cdot p]} \quad \underbrace{\boldsymbol{e} \stackrel{\Delta}{=} \begin{bmatrix} \boldsymbol{e}_1 \\ \boldsymbol{e}_2 \\ \vdots \\ \boldsymbol{e}_M \end{bmatrix}}_{[NM \times 1]}$$

Parameter estimation (determination of the parameter vector $\overline{\boldsymbol{\theta}}$) may be then based upon the Ordinary Least Squares (OLS) criterion:

$$J \stackrel{\Delta}{=} \text{Trace}\, \widetilde{\text{Cov}}[\boldsymbol{e}] = \sum_{k=1}^{M} \sum_{t=1}^{N} e_k^2[t] \tag{18}$$

in which $\widetilde{\mathrm{Cov}}[\cdot]$ designates sample covariance of the indicated vector. This leads to the estimators:

$$\hat{\boldsymbol{\theta}} = \left(\boldsymbol{\Phi}^T\boldsymbol{\Phi}\right)^{-1}\cdot\boldsymbol{\Phi}^T\boldsymbol{y} = \\ = \left[\sum_{k=1}^{M}\sum_{t=1}^{N}\boldsymbol{\phi}_k[t]\boldsymbol{\phi}_k^T[t]\right]^{-1}\cdot\left[\sum_{k=1}^{M}\sum_{t=1}^{N}\boldsymbol{\phi}_k[t]\,y_k[t]\right] \quad (19)$$

$$\hat{\sigma}_e^2(k) = \frac{1}{N}\sum_{t=1}^{N}\hat{e}_k^2[t] \qquad \text{for } k = k_1,\ldots,k_M \quad (20)$$

The $\hat{\boldsymbol{\theta}}$ estimator is asymptotically ($N\to\infty$) Gaussian distributed with mean coinciding with the true parameter vector and covariance matrix $\boldsymbol{P}_\theta$, based upon which interval estimates of the true parameter vector may be constructed [14].

4.2 Fault detection, localization, and estimation (inspection phase)

Let $x[t], y[t]$ ($t = 1,2,\ldots,N$) represent the excitation and response signals, respectively, obtained from the system in its *current* (unknown) state.

Fault detection. Fault detection may be based upon the *re-parametrized* FNARX model of *any* fault mode. Toward this end consider the re-parametrized (in terms of k, σ_e^2, which are the parameters to be estimated) FNARX model corresponding to the stiffness k_2 fault mode [notice that the basis functions and coefficients of projection are those of the chosen fault mode model; compare with equations (9) and (12)]:

$$\mathcal{M}(k,\sigma_e^2):\quad y[t] = \boldsymbol{\varphi}^T[t]\cdot\boldsymbol{\vartheta}(k) + e[t] = \\ = \left[\boldsymbol{\varphi}^T[t]\otimes\boldsymbol{g}^T(k)\right]\cdot\boldsymbol{\theta} + e[t] \quad (21)$$

The estimation of k, σ_e^2 based upon the current excitation and response signals is achieved via the nonlinear regression (Nonlinear Least Squares – NLS) estimator (realized via golden search and parabolic interpolation [15]):

$$\hat{k} \triangleq \arg\min_k \sum_{t=1}^{N} e^2[t] \qquad \hat{\sigma}_e^2 = \frac{1}{N}\sum_{t=1}^{N}\hat{e}^2[t] \quad (22)$$

This estimator may be shown [14] to be asymptotically ($N\to\infty$) Gaussian distributed, with mean equal to the true (underlying) k value, say k^o, and variance σ_k^2 [$\hat{k}\sim\mathcal{N}(k^o,\sigma_k^2)$]. This may be in turn estimated as:

$$\hat{\sigma}_{\hat{k}}^2 = \frac{\hat{\sigma}_e^2}{N}\left[\frac{1}{N}\sum_{t=1}^{N}\left[\frac{\vartheta\hat{e}[t]}{\vartheta k}\right]^2_{k=\hat{k}}\right]^{-1} = \\ = \frac{\hat{\sigma}_e^2}{N}\left[\frac{1}{N}\sum_{t=1}^{N}\left[\boldsymbol{\varphi}^T[t]\otimes\frac{\vartheta\boldsymbol{g}^T(k)}{\vartheta k}\bigg|_{k=\hat{k}}\cdot\hat{\boldsymbol{\theta}}\right]^2\right]^{-1} \quad (23)$$

with $\boldsymbol{\varphi}[t]$ defined by equation (3) and $\hat{\boldsymbol{\theta}}$ designating the chosen fault mode's vector of coefficients of projection [of the form of equation (14)].

Since the healthy system corresponds to $k = 0$, fault detection may be based upon the hypothesis testing problem:

H_0: $k^o = 0$ (No fault has occurred).
H_1: $k^o \neq 0$ (A fault has occurred).

which (based upon the previous results) leads to the following test at the $\alpha = 0.05$ risk level (0.05 probability of type I error, that is rejecting H_0 if it is correct):

Fault detection test ($\alpha = 0.05$)		
$\lvert\hat{k}\rvert \le 1.96\hat{\sigma}_k$	$\Longrightarrow$	H_0 is accepted (no fault is detected).
Else	$\Longrightarrow$	H_0 is rejected (a fault is detected).

Fault identification. Once fault occurrence has been detected, fault localization is based upon the successive estimation and validation of the re-parametrized FNARX models [of the form of equation (21)] corresponding to the various fault modes. The procedure stops as soon as a particular model is successfully validated; the corresponding fault mode is then identified as *current*.

Model validation may be based upon statistical tests examining the hypothesis of excitation and residual sequence uncrosscorrelatedness, as well as residual uncorrelatedness. The latter is presently examined via the statistical hypothesis testing problem:

H_0: $\rho_1 = \rho_2 = \cdots = \rho_h = 0$
(the fault mode is identified as current).
H_1: Some $\rho_i \neq 0$ $(1 \le i \le h)$
(the fault mode is not the current one).

in which ρ_i ($i = 1,2,\ldots,h$) designates the residual series normalized autocorrelation at lag i. It may be shown [16, p. 149] that the test statistic:

$$Q = N\cdot(N+2)\cdot\sum_{i=1}^{h}\frac{\hat{\rho}_i^2}{N-i} \quad (24)$$

in which N designates the residual signal length (in number of samples), $\hat{\rho}_i$ the sample normalized residual autocorrelation, and h the maximum lag, follows

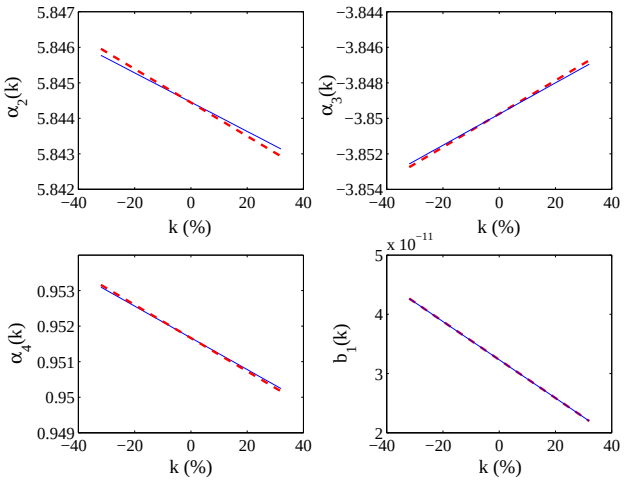

Figure 4: Theoretical (- - -) and FNARX estimated (—) model parameters as functions of the fault magnitude k (fault mode $F_k^{k_2}$).

Test Case	Incurred Fault
I	No fault (healthy system)
II	$F_3^{k_2}$ (3% reduction in stiffness k_2)
III	$F_{29}^{k_2}$ (29% reduction in stiffness k_2)
IV	$F_{30}^{k_1}$ (30% reduction in stiffness k_1)

Table 4: The four test cases.

a chi-square (χ^2) distribution with $h-1$ degrees of freedom.

This leads to the test (at the α risk level):

Fault identification test		
$Q < \chi^2_{1-\alpha,h-1}$	$\Longrightarrow$	H_0 is accepted (fault mode is current).
Else	$\Longrightarrow$	H_0 is rejected (fault mode not current).

Fault magnitude estimation. Once the current fault mode has been determined, the interval estimate of the fault magnitude is constructed based upon Gaussianity and the $\hat{k}$, $\hat{\sigma}_k^2$ estimates [equations (22), (23)] obtained from the $\mathcal{M}(k,\sigma_e^2)$ model [equation (21)] of the identified fault mode. Thus:

Fault magnitude interval estimate ($\alpha = 0.05$):

$$\left[\hat{k} - 1.96\hat{\sigma}_k, \hat{k} + 1.96\hat{\sigma}_k\right]$$

5 Fault detection and identification results

5.1 Baseline and fault mode modeling (a-priori phase).

Baseline modeling. The identification of the baseline (healthy) system via a NARX(na, nb) model of the form of table 3 has been discussed in section 3.

Fault mode modeling. Fault mode modeling is pursued only for the $F_k^{k_2}$ fault mode characterized by changes in the k_2 stiffness (notice that the $F_k^{k_1}$ fault mode is not presently modeled). A total of $M = 17$ experiments, one corresponding to the healthy system ($k = 0\%$ variation in k_2) and the rest corresponding to various fault magnitudes (faults $F_k^{k_2}$ with $k \in [-32, 32\%]$; increment $\delta k = 4\ \%$), are carried out. The signals obtained are, in all cases, $2,000$ $samples$ long.

The FNARX modeling procedure [14] leads to a FNARX(na, nb) $F_k^{k_2}$ fault mode model, with functional basis consisting of the first two (0th and 1st degree, thus $p = 2$) Chebyshev Type II polynomials [17]. The theoretical and FNARX-based estimates of certain of the model parameter trajectories (as functions of the fault magnitude k) are compared in figure 4, from which excellent agreement is observed.

5.2 Fault detection and identification (inspection phase).

Four test cases, as indicated in table 4, are presently considered via Monte Carlo experiments (10 runs per case).

Monte Carlo fault detection results are pictorially presented in figure 5, fault identification (localization) results in figure 6, and a summary of the fault magnitude estimation results (averages over 10 runs per case) is presented in table 5. In all statistical tests the selected risk level is $\alpha = 0.05$. Comments on each test case follow.

Test Case I *(healthy system).* In this case the fault magnitude interval estimate includes the $k = 0$ value in each one of the 10 runs [figure 5(a)], thus *no* fault is (rightly) detected. In addition, the value of the Q statistic is, for all 10 runs, below the critical point [figure 6(a)]. The excellent accuracy of the k estimates is confirmed by the average (over the 10 runs) point and standard deviation estimates presented in table 5.

Test Case II *(fault $F_3^{k_2}$ – 3% reduction in the k_2 stiffness).* This is a small magnitude fault, yet fault detection is accurate in all 10 runs [the fault magnitude

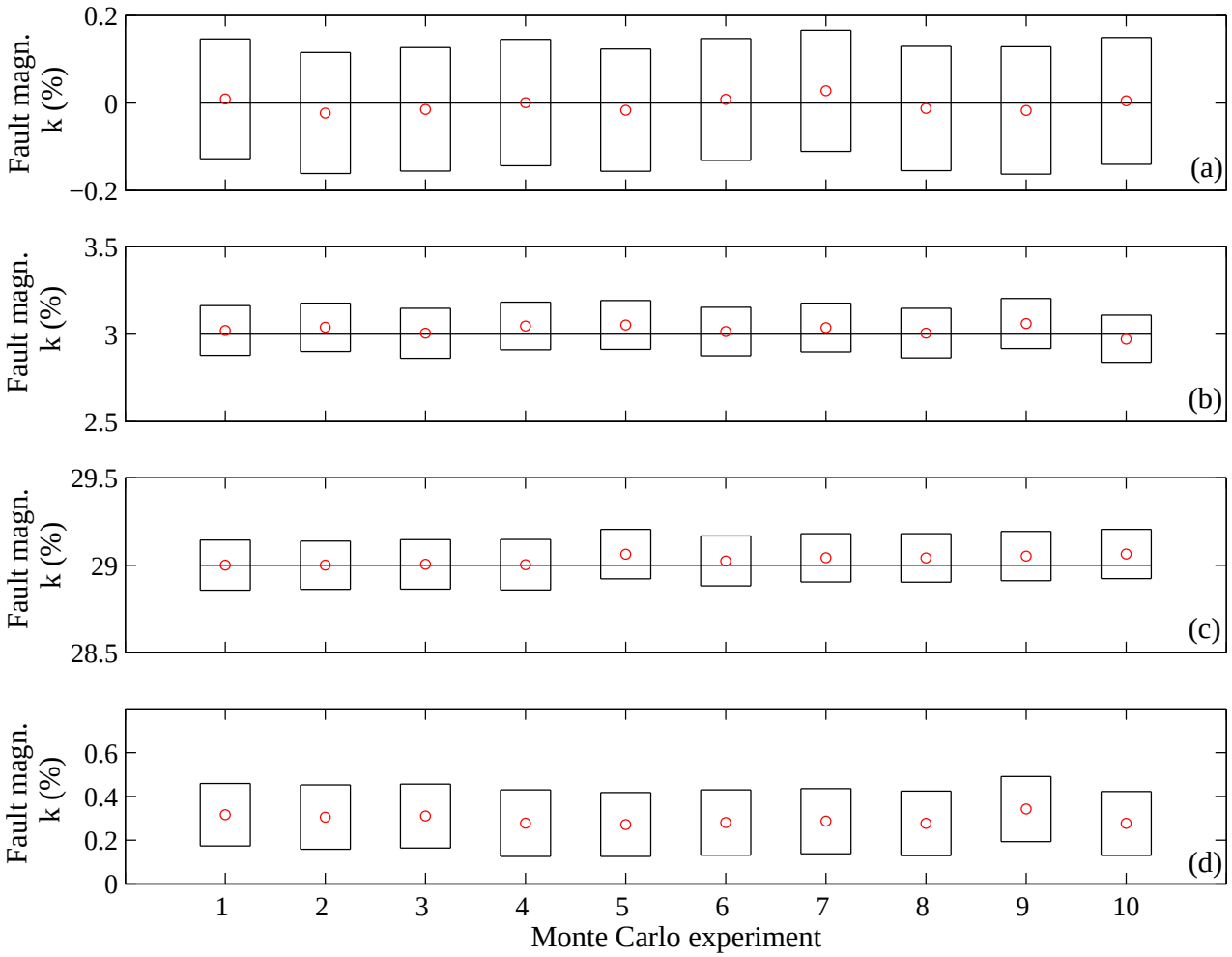

Figure 5: Fault detection results: (a) Test case I (healthy system); (b) test case II (fault $F_3^{k_2}$); (c) test case III (fault $F_{29}^{k_2}$); (d) test case IV (fault $F_{30}^{k_1}$) [10 Monte Carlo runs per case; the solid horizontal lines designate true fault magnitude, the circles corresponding point estimates, and the boxes interval estimates at the $\alpha = 0.05$ level].

Test Case	Fault	True Fault Magnitude k^o (%)	Average Point Estimate $\overline{\hat{k}}$	Average Standard Deviation Estimate $\overline{\hat{\sigma}}_k$
I	$F_0^{k_2}$	0	-2.59×10^{-3}	7.20×10^{-2}
II	$F_3^{k_2}$	3	3.02	7.12×10^{-2}
III	$F_{29}^{k_2}$	29	29.02	7.18×10^{-2}

Table 5: Fault magnitude estimation results (averages over 10 Monte Carlo runs).

interval estimates do not include the $k = 0$ value; figure 5(b)]. The $F_k^{k_2}$ fault mode is also correctly identified, as the value of the Q statistic is, for all 10 runs, below the critical point [figure 6(b)]. The excellent accuracy of the k estimates is, once again, confirmed by the average (over the 10 runs) point and standard deviation estimates presented in table 5.

Test Case III *(fault $F_{29}^{k_2} - 29\%$ reduction in the k_2 stiffness)*. This is a larger magnitude fault, the detection of which is also without problems in all 10 runs [the fault magnitude interval estimates do not include the $k = 0$ value; figure 5(c)]. Fault mode identification is also accurate, as the value of the Q statistic is below the critical point for all 10 runs [figure 6(c)].

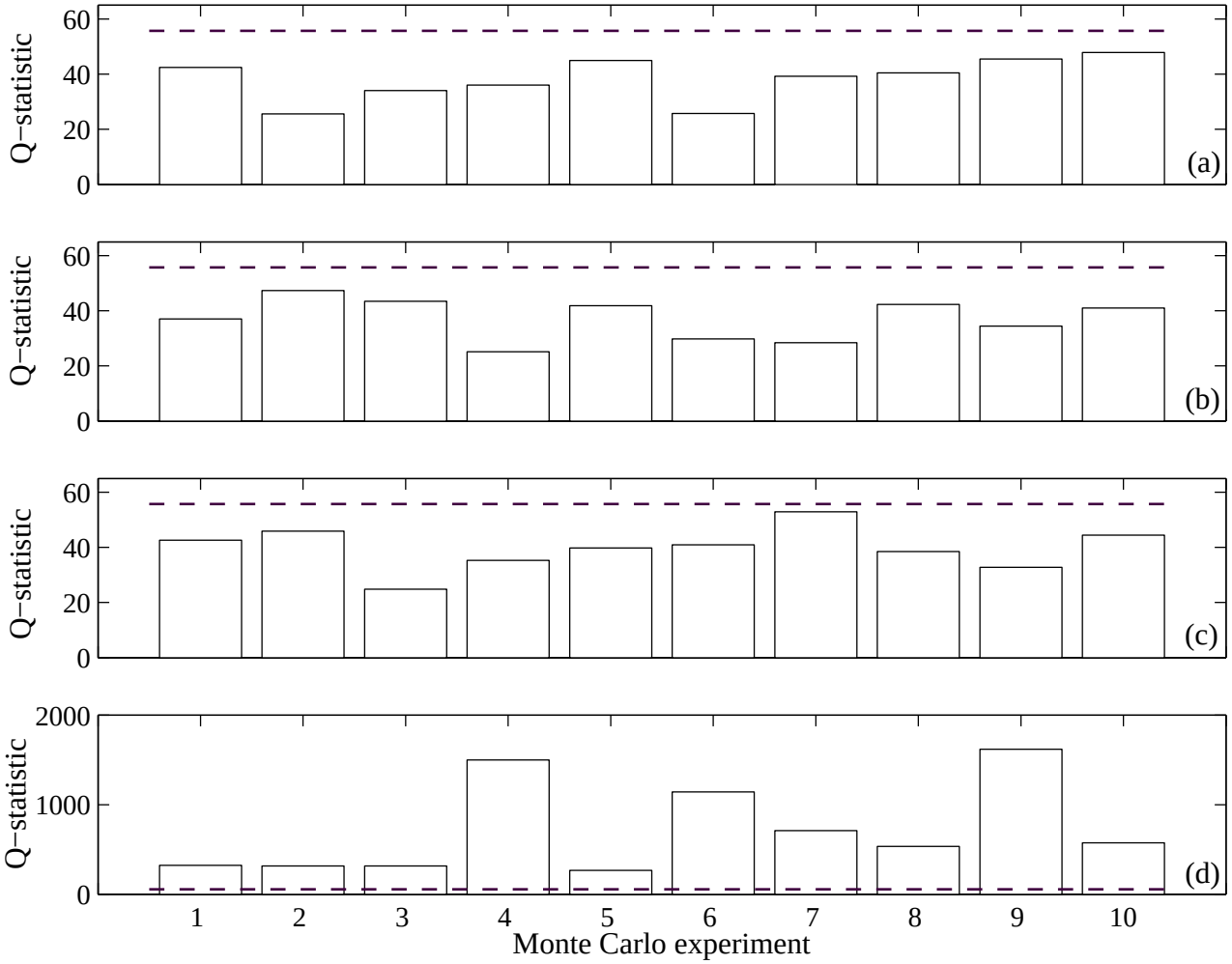

Figure 6: Fault identification results: Q statistic (bars) and the critical point (- - -) at the $a = 0.05$ level (the fault mode $F_k^{k_2}$ is identified as current if Q is lower than the critical point). (a) Test case I (healthy system); (b) Test case II (fault $F_3^{k_2}$); (c) test case III (fault $F_{29}^{k_2}$); (d) test case IV (fault $F_{30}^{k_1}$) [10 Monte Carlo runs per case; $h = 40$].

The accuracy of the k estimates is similarly excellent (table 5).

Test Case IV *(fault $F_{30}^{k_1}$ – 30% reduction in the k_1 stiffness).* This is a somewhat different case, as the fault considered does *not* belong to the modeled $F_k^{k_2}$ fault mode (for this reason fault magnitude estimation is not addressed).

Yet, the obtained fault detection results are very good, as the fault magnitude interval estimates do not, in all 10 runs, include the $k = 0$ value [figure 5(d)]. Moreover, the fault mode identification results definitely suggest that the present fault does not belong to the $F_k^{k_2}$ mode, as the value of the Q statistic is far above the critical point for all 10 runs [figure 6(d)].

6 Conclusions

This paper was concerned with system identification and fault detection in a two DOF nonlinear system characterized by cubic stiffness. System identification was based upon Nonlinear ARX (NARX) models, while a novel Functional Model Based Method, using Functional NARX (FNARX) models, was, for the first time, employed for fault detection, identification, and fault magnitude estimation within the context of a nonlinear system.

The results of the study confirmed: (a) The effectiveness and accuracy of NARX based identification for the system at hand; (b) the effectiveness and accuracy of the Functional Model Based Method for tackling the combined problem of fault detection, identification, and fault magnitude estimation.

The Functional Model Based Method was specifically demonstrated to accurately detect, identify (localize), and estimate even small magnitude faults (a fault as small as 3% stiffness reduction was considered) in the presence of stochastic uncertainty and only two measured signals.

Acknowledgements

The authors acknowledge the financial support of this study in part by the General Secretariat for Research and Technology – Greece and the European Social Fund (PENED99 Project #580), and in part by the European Commission (Growth Project GRD1-2000-25261 – ADFCSII).

References

[1] K. Worden, G.R. Tomlinson, *Nonlinearity in Structural Dynamics: Detection, Identification and Modeling*, Institute of Physics Publishing, 2001.

[2] I.J. Leontaritis, S.A. Billings, *Input-output parametric models for non-linear systems: parts I and II*, Intl. Journal of Control, Vol. 41(2), Taylor and Francis Ltd (1985), pp. 303-344.

[3] P. Palumbo, L. Piroddi, *Harmonic analysis of non-linear structures by means of generalized frequency response functions coupled with NARX models*, Mechanical Systems and Signal Processing, Vol. 14(2), Academic Press (2000), pp. 243-265.

[4] L. Ljung, *System Identification: Theory for the User*, Second Edition, Prentice Hall PTR (1999).

[5] S.D. Fassois, *Parametric Identification of Vibrating Structures*, in *Encyclopedia of Vibration*, S.G. Braun, D.J. Ewins, S.S. Rao, editors, Academic Press (2001), pp. 673-685.

[6] A.A. Khan, N.S. Vyas, *Non-linear parameter estimation using Volterra and Wiener theories*, Journal of Sound and Vibration, Vol. 221(5), Academic Press (1999), pp. 805-821.

[7] A.A. Khan, N.S. Vyas, *Nonlinear bearing stiffness parameter estimation in flexible rotor-bearing systems using Volterra and Wiener approach*, Probabilistic Engineering Mechanics, Vol. 16, Elsevier Science Ltd (1999), pp. 137-157.

[8] Y. Benhafsi, J.E.T. Penny, M.I. Friswell, *A parameter identification method for discrete non-linear systems incorporating cubic stiffness elements*, Intl. Journal of Analytical and Experimental Modal Analysis, Vol. 7(3) (1992), pp. 179-195.

[9] S. Chen, S.A. Billings, W. Luo, *Orthogonal least squares methods and their application to non-linear system identification*, Intl. Journal of Control, Vol. 50, Taylor and Francis Ltd (1989), pp. 1873-1896.

[10] J.S. Sakellariou, D.D. Rizos, S.D. Fassois, *Fault detection and magnitude estimation for an aircraft skeleton structure via a Functional Model Based Method*, *First European Workshop on Structural Health Monitoring, Paris, France*, (2002), in press.

[11] J.S. Sakellariou, K.A. Petsounis, S.D. Fassois, *On board fault detection and identification in railway vehicle suspensions via a Functional Model Based Method*, *Proceedings of ISMA 2002, Leuven, Belgium*.

[12] A.J. Jerri, *Linear Difference Equations With Discrete Transform Methods*, Kluwer Academic Publishers (1996).

[13] J.R. Magnus, H. Neudecker, *Matrix Differential Calculus*, John Wiley and Sons (1988).

[14] J.S. Sakellariou, S.D. Fassois, *Stochastic dynamical functional models: properties and estimation*, under preparation for publication (2002).

[15] G.E. Forsythe, M.A. Malcolm, C.B. Moler, *Computer Methods for Mathematical Computations*, Prentice-Hall (1976).

[16] W.W.S. Wei, *Time Series Analysis: Univariate and Multivariate Methods*, Addison-Wesley Publishing Company (1990).

[17] M. Abramowitz, I.A. Stegun, *Handbook of Mathematical Functions*, Dover (1970).